ISSN (Print) 1226-1750
ISSN (Online) 2233-6656
Journal of Magnetics 25(4), 540-546 (2020) https://doi.org/10.4283/JMAG.2020.25.4.540

Bimodal Approach for the Use of Co Doped Magnetite as MRI Contrast Agent and Potential Antitumor

Ahmed. A. G. El-Shahawy[1]*, Yasser GadelHak[1], H. Y. Zahran[2,3], I. S. Yahia[2,3], and S. I. El-Dek[1]

[1]*Materials Science and nanotechnology Dept., Faculty of Postgraduate Studies for Advanced Sciences (PSAS), Beni-Suef University, Beni-Suef, Egypt*
[2]*Research Center for Advanced Materials Science (RCAMS), King Khalid University, Abha 61413, P.O. Box 9004, Saudi Arabia*
[3]*Metallurgical Lab., Nanoscience Laboratory for Environmental and Bio-medical Applications (NLEBA), Semiconductor Lab., Physics Department, Faculty of Education, Ain Shams University, Roxy, 11757 Cairo, Egypt*

(Received 5 September 2020, Received in final form 24 December 2020, Accepted 24 December 2020)

Cobalt doped magnetite $Co^{2+}_{0.1}Fe^{2+}_{0.9}Fe^{3+}_{2}O_4$ nanocrystals were synthesized chemically using simple one step coprecipitation in the absence and presence of the magnetic field. The nanocrystals were characterized by transmission electron microscopy (TEM), X-ray diffraction (XRD), magnetization studies by vibrational spectroscopy magnetometer (VSM). The signal intensity of the prepared nanoparticles was measured by magnetic resonance imaging (MRI). The cytotoxicity of the two samples versus W138 normal lung cells and AS49 lung cancer cells was investigated by MTT assay, *in vitro*. The TEM images showed non-spherical and aggregated nanoparticles, heterogeneously dispersed with 100 nm average size. The XRD and selected area electron diffraction of the two samples revealed good crystallinity for both samples. The room temperature magnetization curves demonstrate the general ferrimagnetic trend with a clear difference in the coercivity and the remanence keeping the saturation magnetization nearly stable. The measured MR signal intensity was well-matched with the result of the M-H loops where the sample prepared in the absence of the field was a promising T2 contrast agent. Both samples have low cytotoxicity compared to Doxorubicin.

Keywords : cobalt doped magnetite, magnetic field, contrast agent, cytotoxicity, lung cancer

1. Introduction

Magnetic nanoparticles (MNPs), precise rule over the formation, and stability are crucial. Among the MNPs, nanosized ferrites magnetic materials are the substances of intensive investigation work; because of their diverse applications in different fields such as magnetic disc drives, spintronics, ferrofluids, catalysts, medical diagnostics, drug delivery systems, pigments in paints, and ceramics [1, 2]. The high resistivity and low hysteresis loss of ferrites are suitable to use in microwave applications and radio electronics. The ferrites with the general formula MFe_2O_4 have been used in many applications [3, 4]. By adjusting the M^{2+} cations, several studies on pure nano ferrites such as Fe_3O_4, $NiFe_2O_4$, $CoFe_2O_4$, $ZnFe_2O_4$, and $MnFe_2O_4$ have demonstrated the interplay of composition, cations distribution, and size, in view of their properties and applications [5, 6]. Among the ferrites, $CoFe_2O_4$ has received significant attention in recent years, and the most important and interesting oxides owing to their wide variety of applications in sensors, electronics, and catalysts [7, 8].

Different methods are used to prepare $CoFe_2O_4$ as electrochemical methods, hydrothermal methods, co-precipitation, mechanical milling, sol-gel methods, or precipitation in a polymer matrix [9, 10]. In spite of the availability of different synthetic methods and promising potential applications, the synthesis of high monodisperse and non-aggregated $CoFe_2O_4$ nanoparticles has not been mastered so far [11]. Here we employed a facile and simple method for the synthesis of uniform Co-doped magnetite nanoparticles by using suitable precursors $CoCl_2$, $FeSO_4$, and $FeCl_3$ in the presence and absence of the magnetic field to investigate the effect of the magnetic field on the physicochemical properties of the nanoparticles. We appointed a magnetic field to control the size, and to enhance the magnetic properties overall without any change in the composition. Moreover, this

©The Korean Magnetics Society. All rights reserved.
*Corresponding author: Tel: +01226798209
Fax: +01226798209, e-mail: ahmed.elshahawy@psas.bsu.edu.eg

© 2020 Journal of Magnetics

current synthesis method is a short time with no need for special apparatus/conditions and precipitate agents.

2. Materials and Methods

2.1. Materials

2.2. Synthesis of $Co^{2+}_{0.1}Fe^{2+}_{0.9}Fe^{3+}_{2}O_4$

Aqueous solutions of $CoCl_2$, $FeSO_4$, and $FeCl_3$ in their respective stoichiometry were mixed, and NaOH was added within the 30s to the boiling solution, adjusting the pH to 12, while stirring continuously. The Precipitation and formation of nano magnetite occurred by the conversion of metal salts into hydroxides, which is formed immediately, and then followed by the transformation of hydroxides into magnetite. The precipitate was then collected by magnetic decantation and thoroughly washed with double distilled water and then dried. The same procedures were repeated between the 2 poles of the electromagnet with an applied magnetic field 1000 Oe.

2.3. Materials characterization

The crystallinity of the prepared materials was investigated by X-ray Diffractometer (PANalytical Empyrean, Netherlands) with CuKα radiation (40 kV, current 35 mA), scanning range 10-70°, scan step 0:05°, and wavelength λ = 1.54045 Å. The crystallite size (L) was determined from the measurements of the FWHM using Scherrer's formula: $L_{XRD} = 0.9\,\lambda/\beta\cos\theta$ where; β is the corrected full width at half maximum of the line spectrum in radians, θ is Bragg's angle, and λ is the target wavelength. TEM micrographs were taken using JEOL JSM-1230 on a copper-coated carbon grid. Zeta potential was measured using (Malvern Instruments Ltd). The room temperature magnetic hysteresis of samples was measured up to a maximum field of 20 kOe using vibrating sample magnetometer (VSM) model 9600–1 LDJ, USA.

2.4. MR signal intensity measurements in T2 weighted images

A clinical 1.5 Tesla MRI scanner (Magnetom era, Siemens Medical Solutions, Erlangen, Germany) and an 8-channels wrist transceiver coil were employed. For measuring the MR signal intensity of the prepared $Co^{2+}_{0.1}Fe^{2+}_{0.9}Fe^{3+}_{2}O_4$ nanoparticles, the prepared samples were dispersed separate, in a falcon tube 15 ml that contained liquid phantom with a concentration of 0.5 mM. T2 weighted imaging of the two samples occurred simultaneously, with the same parameters. The imaging parameters were: a multi-echo spin-echo pulse sequence with a total of 32 echos, and Repetition time TR = 5000 ms was used, the echo time TE was 224 ms, slice thickness = 1 mm, the field of view (FOV) = 50 × 50 mm, matrix = 256 × 256, and flip angle (FA) = 180.0°.

2.5. In vitro cytotoxicity

The cytotoxicity of $Co^{2+}_{0.1}Fe^{2+}_{0.9}Fe^{3+}_{2}O_4$ nanoparticles versus WI38 normal lung cells and A549 Lung cancer cells was measured by MTT assay, in vitro. The cells were first cultured in a 96-well plate with DMEM for 24 hours and then starved for 6 hours. Next, the cells were treated with different concentrations of nanoparticles (0-100 μM) in the cell medium. After 48 hours of incubation, MTT was added to each well to a final concentration of 0.5 mg/mL and incubated for another 4 hours. The solution was discarded, and 150 μL of DMSO was added to each well. Absorbance was measured with a microplate reader (Bio-Rad Model 680, Hercules, CA, USA) at 570 nm [12].

3. Results and Discussion

3.1. $Co^{2+}_{0.1}Fe^{2+}_{0.9}Fe^{3+}_{2}O_4$ nanoparticles: synthesis and structure

The TEM images showed the presence of non-spherical and aggregated nanoparticles heterogeneously dispersed with no significant difference between the two samples. The size distribution as measured by TEM showed that the mean size value of the nanoparticles is centered at 50 nm, as shown in Fig. 1, 2. There is no great difference

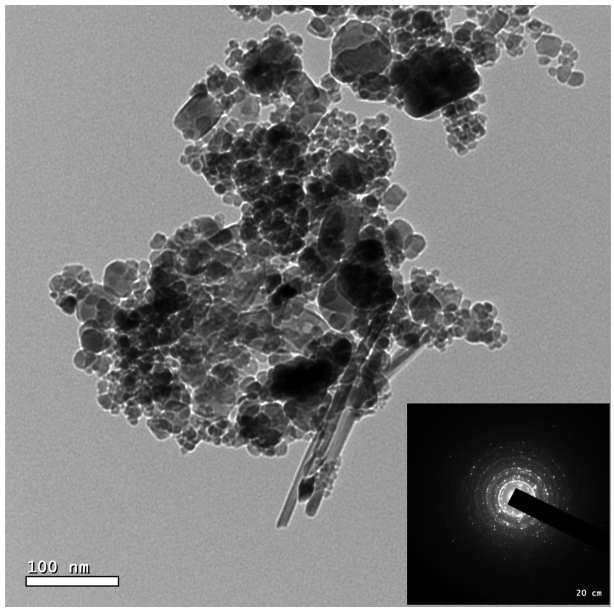

Fig. 1. The transmission electronic microscopy (TEM) measurements performed for the prepared nanoparticles in the presence of the magnetic field. The inset is the SAED image.

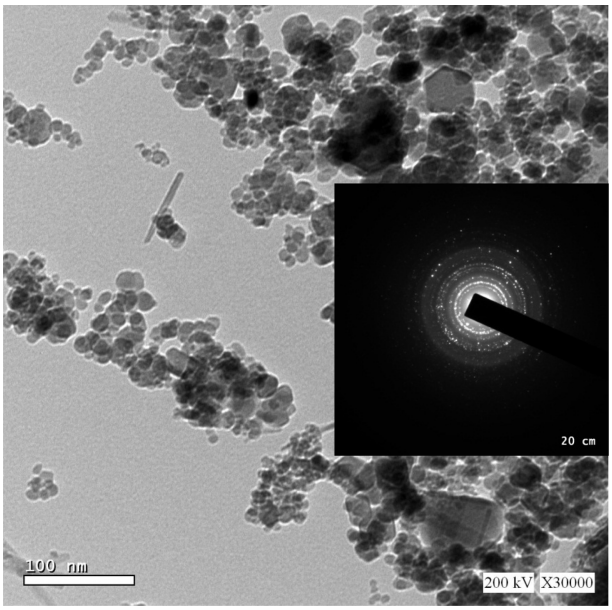

Fig. 2. The transmission electronic microscopy (TEM) measurements performed for the prepared nanoparticles in the absence of the magnetic field. The inset is the SAED image.

between the two samples. Only the sample prepared in the presence of a magnetic field has more elongated particles than spherical ones. The magnetic field here was not high enough to produce effective particle shape changes. However, its effect is to reorient some particles during the growth under alkaline conditions. The selected area electron diffraction of the two samples revealed concentric rings well seen pointing to the good crystallinity of both, which was confirmed by the XRD patterns.

The XRD, Fig. 3 showed a good crystallinity of the two samples. The XRD pattern matched with the magnetite standard diffraction peaks reported in the [ICDD card 00-001-1111]. The peaks at angles of 30.3°, 35.7°, 37.2°, 43.3°, 53.7°, 57.1°, and 62.9° were indexed to the (220), (311), (222), (440), (422), (511) and (440) plane families, respectively. The observed intensities matched-well with the cubic structure of $Co^{2+}_{0.1}Fe^{2+}_{0.9}Fe^{3+}_{2}O_4$; no other phases were detected, indicating the single phase of the prepared $Co^{2+}_{0.1}Fe^{2+}_{0.9}Fe^{3+}_{2}O_4$, and no noise peaks were observed, reflecting the phase purity. A small unindexed peak is observed at about 45.1° with a very small intensity within the background.

The XRD analysis provided information about crystallite size, which was estimated by deconvolution of the peak-broadening within the framework of the fundamental parameter approach. By considering the most intense (311) peak of XRD, the crystallite size of the samples is calculated from the diffraction peak in the XRD profile,

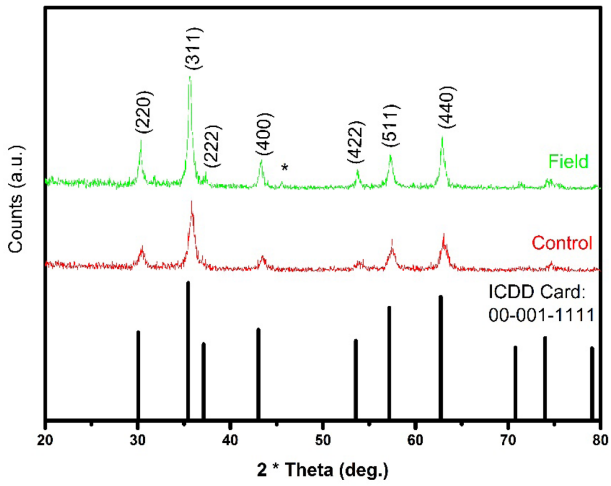

Fig. 3. (Color online) XRD of the prepared samples.

in accordance with Debye-Scherer's formula $L = \frac{0.89\lambda}{\beta\cos\theta}$.

Where, L, λ, β, and θ are the average crystallite size, X-ray wavelength (0.1542 nm), the corrected full width at half maximum (FWHM), and the Bragg angle of the (311) plane, respectively. The computed crystallite size for the control and field samples was 17 nm and 35 nm, respectively. The values reflected that the presence of a magnetic field in the co-precipitation state, enhanced the long-range order of atoms in the formed crystallites, compared to the control sample. It was worth referring that the crystallite sizes were in good agreement with the values obtained from TEM analysis. Besides, the crystallographic parameters of the field sample revealed a cubic crystal system with a space group of p4332 and space group number 212. The lattice parameter (a, b & c) were equal to 8.3364 Å, and ($\alpha = \beta = \gamma$) equal to 90°. The non-field sample, exhibited the same crystallographic parameters while the lattice (a, b & c) parameters increased to equal 8.3416 Å. The recorded lattice space of the field sample revealed a linear decrease of the d-spacing compared to the non-field sample.

In the FTIR spectrum Fig. 4, the transmittance bands at around 575 cm^{-1} and 395 cm^{-1} can be attributed to the Fe-O bond [13]. These bands can be assigned to the Fe–O stretching mode of the tetrahedral and octahedral sites (the band at 575 cm^{-1}) and to the Fe–O stretching mode of the octahedral sites (the band at 395 cm^{-1}).The band at 1600 cm^{-1} and that at 3380 cm^{-1} is due to the OH groups bending and stretching, which originated from the adsorbed water molecules [14].

The control and field samples showed a zeta potential of 10.8 and 8.3 mV, respectively. The low zeta potential values explained the aggregation state of the prepared

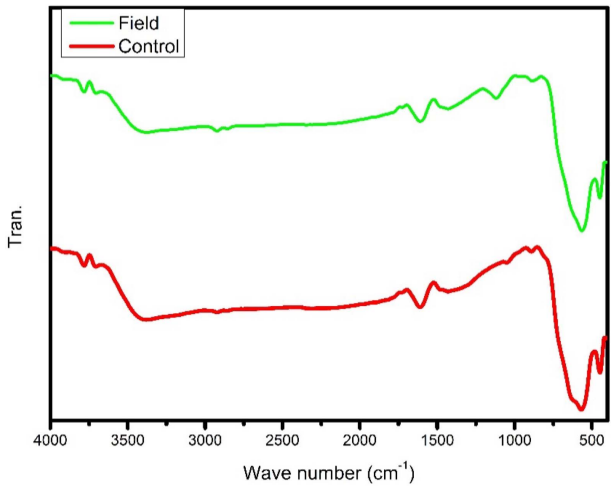

Fig. 4. (Color online) FTIR spectra of the prepared samples.

nanoparticles that appeared in the TEM images, which is mainly due to magnetostatic interaction between magnetic nanoparticles below 50 nm.

3.2. Magnetism

It is well known that the magnetic properties of materials are characterized by their hysteresis loops. The magnetic properties of the prepared samples have been determined at room temperature using a vibrating sample magnetometer (VSM) in the applied magnetic field up to 20 kOe. Figure 5 is the VSM of the powdered-nanocrystalline prepared samples, with and without a magnetic field. The plotted Hysteresis loops displayed the variation of magnetization (M_s, emu/g) as a function of the applied magnetic field (H, Oe). Overall, the first zone is nonlinear, and the rate of change of M_s concerning increasing in H is increasing, which means increasing the value of H

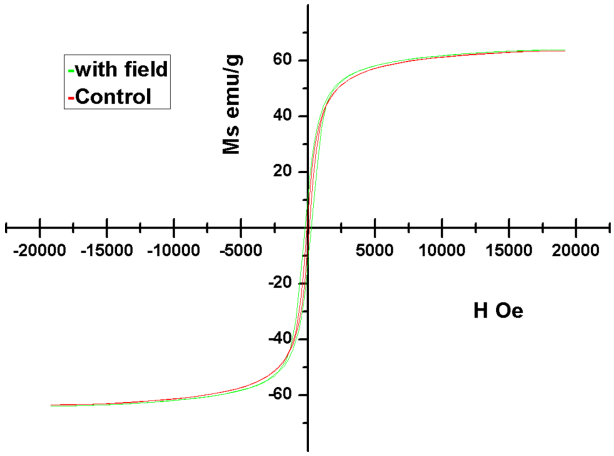

Fig. 5. (Color online) M-H loop of the prepared samples, with and without magnetic field.

increases the magnetization rapidly. Before the saturation region, the rate of increase of M_s with respect to increasing in H is very slow. Further increasing magnetic field intensity leads to the well-known plateau of saturation.

There was a change in the magnetic parameters namely in remanent or retentively magnetization (M_r), and coercivity (H_c), but there is no significant variation in the saturation magnetization. The measured magnetic parameters of the field sample were H_c 226.31G, M_s 63.931 emu/g, and M_r 11.451 emu/g, while those of the non-field sample revealed H_c 84.667G, M_s 63.469 emu/g, and M_r 5.2510 emu/g. Here the coercivity of the nanoparticles prepared in the presence of the magnetic field exhibited a nearly triple value of H_c and double the remanence as compared with that synthesized without file. These variations are mainly based on the distribution of the Fe^{+2} and Fe^{+3} ions among the lattice sites or in the crystals. Hence, one can say that using the magnetic field during the preparation varied and controlled the distribution of the Fe^{+2} and Fe^{+3} ions and their arrangement. Co^{2+} substituted Fe^{2+} ions on the octahedral sites of the magnetite spinel matrix as it is known to be an inverse spinel $Fe^{3+}[Fe^{2+}Fe^{3+}]O_4$. Another reason behind the increase in Hc and Mr keeping the saturation unchanged is that Co is known to have positive magneto-crystalline anisotropy and the magnetic field used during preparation was less than half that causing the onset of saturation. Additionally, the increase in crystallite size (35 nm), which is double that without field is the main reason for the enlargement of the Hc. There are two techniques to improve the coercivity of the magnetic nanoparticles either by enhancing the acicular form, which increases the shape anisotropy, or by increasing the magneto-crystalline anisotropy [15, 16].

The two samples are soft where the Squareness ratio (SQR) is 0.17 in case of the present magnetic field while the control sample has SQR = 0.08. Both values indicate the magnetostatic interaction between nanoparticles, this means that both samples were easy to demagnetize, and the enclosed small area of the hysteresis loop has demonstrated and supported these findings. Hence, one can say that the prepared samples displayed the characters of soft magnetic materials, and the magnetic field value is not quite enough to generate pronounced changes in the grain growth and/or shape. An only a small fraction of elongated nanoparticles in the form of nanotubes appeared clear in the sample prepared in the presence of the magnetic field. Consequently, this leads to an enlarged anisotropy by the contribution of shape anisotropy, in addition to the magneto-crystalline one. This in turn is reflected as larger coercivity and remanence. The relationship between particle

size and the magnetic parameters, such as the coercivity (*Hc*), of Fe_3O_4 NPs was reported in different cases for different particle shapes. The critical size of magnetic NPs, which points to the transition from a single to multi-domain structure, was estimated from the variation of *Hc* with the particle size. The particle size needed to achieve super-paramagnetism in Fe_3O_4 NPs is estimated to be ≤ 20 nm [17, 18, 19]. On the other hand, the theoretical critical size for multi-domain structure formation was 76 nm for cubic and 128 nm for spherical magnetite NPs. For cubic magnetite nanocrystals, the multidomain was depicted to be > 160 nm [20]. In our case, both samples are single domain but did not reach super-paramagnetism.

3.3. MR signal intensity

In the world of MR imaging, it is well known that the used contrast agent either be positive or negative [20]. In other words, the positive contrast agent is usually used in the T1 weighted image displaying bright signal intensity or hyper-intensity, which in turn reflects the protons relaxation time in the region of interest, after switching off the Radiofrequency RF excitation source, in another meaning indicates the recovery of the longitudinal magnetization. On the other hand, the negative contrast agent is usually used in the T2 weighted image displaying dark signal intensity or hypo-intensity, which in turn emulates the decay of the transverse magnetization in the region of interest. To evaluate the effect of the presence and absence of the magnetic field on the prepared magnetite to be used as a contrast agent in MRI, the decay of the transverse magnetization would be estimated as a degree of darkness in T2 the weighted image. Figure 6 displays T2 weight images of the two samples; in synchronized acquisition imaging, the upper of the image was the prepared sample in the absence of the magnetic field, while the lower was that prepared in the presence of the magnetic field. The figure revealed a variation in the signal intensity, which represented as the difference of the blacking degree (arrowhead). After switching off the RF, the decay of the transverse magnetization of the prepared nanoparticles in the absence of magnetic field was fast (i.e. loss of magnetization), and hence the value of the measured signal intensity on the transverse magnetization was low resenting dark signal intensity. In complete contrast, the decay of the transverse magnetization of the prepared Co-doped magnetite in the presence of the magnetic field was slow, and hence the value of the measured signal intensity on the transverse magnetization was high resenting bright signal intensity (arrowhead). It is worth noting that the decayed measured MR signal

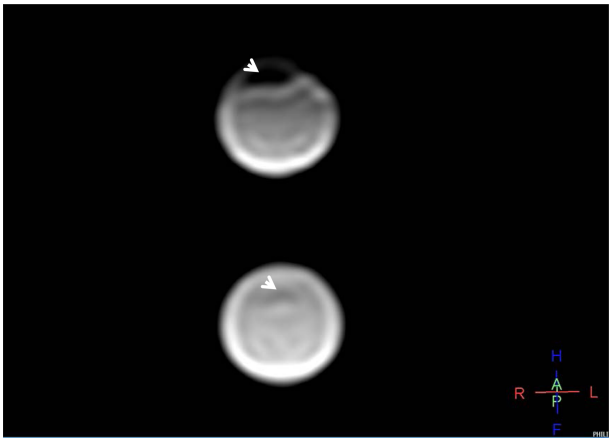

Fig. 6. (Color online) T2 weight image of the two samples; in synchronized acquisition imaging, the upper of the image was the prepared sample in the absence of the magnetic field, while the lower was that prepared in the presence of the magnetic field.

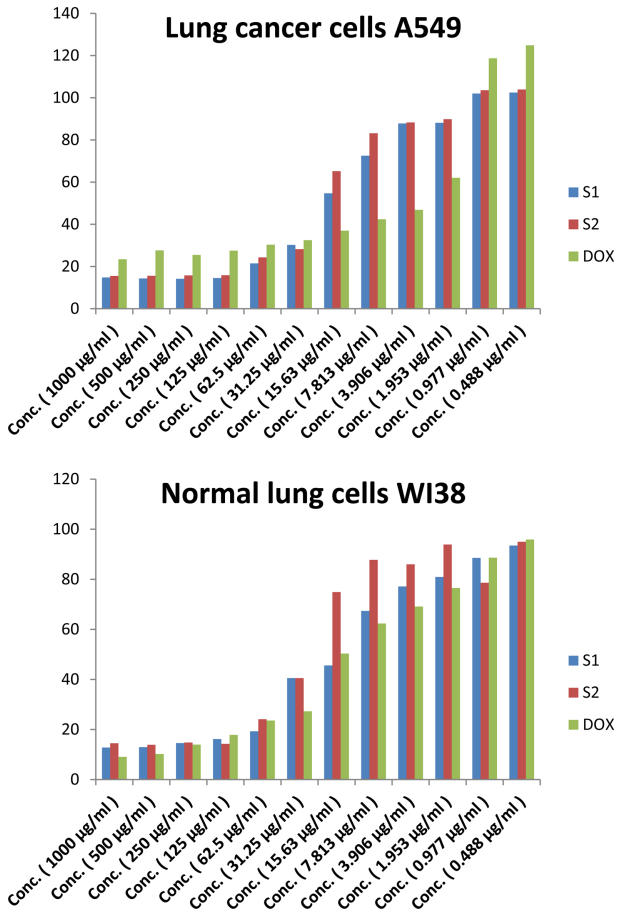

Fig. 7. (Color online) Relative viabilities of WI38 normal lung cells, A549 Lung cancer cells incubated with various concentrations of the prepared sample S1 = prepared in presence of magnetic field & S2 in absences: Data are expressed as means ± SD of four independent experiments. The standard reference was Doxorubicin DOX drug.

intensity was well-matched with the result of the VSM, which revealed that the magnetization retentively of the field prepared sample was higher than that of the non-field sample. The control nanoparticle ($Co^{2+}_{0.1}Fe^{2+}_{0.9}Fe^{3+}_{2}O_4$) in the absence of the field was a promising T2 contrast agent despite their single domain nature.

3.4. In vitro toxicity

The biocompatibility of the prepared for prepared $Co^{2+}_{0.1}Fe^{2+}_{0.9}Fe^{3+}_{2}O_4$ is critical for their potential imaging applications. A previous study indicated that magnetic nanoparticles induced notable pathological changes in the lung, liver, and kidney [14]. Another one reported that magnetic nanoparticles at a high dose were able to cause damage in the liver, kidney, and spleen. Herein, considering the lung toxicity of the prepared $Co^{2+}_{0.1}Fe^{2+}_{0.9}Fe^{3+}_{2}O_4$ either in presence, and absence of magnetic field, was considered, including WI38 normal lung cells, A549 Lung cancer cells. Figure 7 shows the cell viability after 48 hours of incubation with various concentrations of the prepared samples. The IC50 (μg/ml) of the WI38 normal lung cells was, S1 (15.79), S2 (16.86), and DOX (4.46) while that of A549 Lung cancer cells was S1 (15.2), S2 (25.86), and DOX (32). Although the viability of each type of cell at all tested concentrations showed a significant difference, and each sample revealed a cytotoxic effect on normal and cancer cells; nevertheless, the slight difference between S1 and S2 where S2 revealed larger values of viable cells than that exposed to S1. Besides, both samples have low cytotoxicity compared to Doxorubicin which could orient us to use these nanoparticles in drug conjugation/ delivery with the aid of a small external magnetic field. Another additional potential application is their use in magnetic hyperthermia conjugated with the suitable anticancer drug with a low dose.

4. Conclusion

Co-doped magnetite nanoparticles were chemically synthesized in the absence and presence of magnetic. FTIR studies confirmed the molecular structure, and XRD revealed good crystallinity. The HRTEM image displayed the average particle size 50 nm, in agreement with XRD measurements. The magnetization curves demonstrate that the investigated nanoparticles at room temperature tend to be ferrimagnetic with clear saturation. Only, the absence field sample exhibited a strong T2 decay signal as a contrast agent in MRI. However, the existence of valuable coercivity hinders the clinical setting; it should be the superparamagnetic candidate. Future work on the decrease of agglomeration using suitable biocompatible capping could lead to perfect super-paramagnetism. Besides, no significant difference was detected at the cytotoxicity level. In total, the presence of the magnetic field could be used in tuning the magnetic properties of the magnetic nanoparticles. More extensive studies are needed to find out the effect of larger fields on all the microstructure, morphology, and magnetic state of the magnetite as it is biocompatible and of low cytotoxicity.

Acknowledgments

The authors are thankful to all members at Materials Science and nanotechnology Dept., Faculty of Post-graduate Studies for Advanced Sciences (PSAS), Beni-Suef University Egypt for supporting preparation of the nanomaterials. Also, all members at Central Lab for Characterization.

The authors express their appreciation to the Deanship of Scientific Research at King Khalid University for funding this work through research groups program under grant number R.G.P.2/39/40.

References

[1] R. F. Butler and S. K. Banerjee, J. Geophys. Res. **80**, 4049 (1975).
[2] D. L. Huber, Small **1**, 482 (2005).
[3] B. P. Jacob, A. Kumar, R. P. Pant, S. Singh, and E. M. Mohammed, Bull. Mater. Sci. **34**, 1345 (2011).
[4] Y. W. Jun, Y. M. Huh, J. S. Choi, J. H. Lee, H. T. Song, S. J. Kim, S. R. Yoon, K. S. Kim, J. S. Shin, J. S. Suh, and J. W. Cheon, J. Am. Chem. Soc. **127**, 5732, (2005).
[5] M. Kurian and D. S. Nair, J. Saudi Chem. Soc. **20**, 517 (2016).
[6] M. Kurian, S. Thankachan, D. S. Nair, E. K. Aswathy, B. Aswathy, A. Thomas, and K. T. B. Krishna, J. Adv. Ceram. **4**, 199 (2015).
[7] D. L. Leslie-Pelecky and R. D. Rieke, Chem. Mater. **8**, 1770 (1996).
[8] J. Lin, J. Zhang, H. Sun, Q. Lin, Z. Guo, H. Yang, and Y. He, Materials (Basel). **11**, 2095 (2018).
[9] K. Maaz, A. Mumtaz, S. K. Hasanain, and A. Ceylan, J. Magn. Magn. Mater. **308**, 289 (2007).
[10] A. Manikandan, J. Judith Vijaya, M. Sundararajan, C. Meganathan, L. J. Kennedy, and M. Bououdina, Superlattices Microstruct. **64**, 118 (2013).
[11] B. Nakhjavan, M. N. Tahir, M. Panthofer, H. Gao, T. D. Schladt, T. Gasi, V. Ksenofontov, R. Branscheid, S. Weber, U. Kolb, L. M. Schreiber, and W. Tremel, J. Mater. Chem. **21**, 6909 (2011).
[12] K. Nejati and R. Zabihi, Chem. Cent. J. **6**, 23 (2012).
[13] D. Srikala, V. N. Singh, A. Banerjee, and B. R. Mehta, J. Nanosci. Nanotechnol. **10**, 8088 (2010).

[14] C. R. Stein, M. T. S. Bezerra, G. H. A. Holanda, J. André-Filho, and P. C. Morais, AIP Adv. **8**, 056303 (2018).
[15] K. Wang, P. Yang, R. Guo, X. Yao, and W. Yang, Chinese Chem. Lett. **30**, 2013 (2019).
[16] Y. Wang, H. Wei, and Z. Li, Results Phys. **8**, 262 (2018).
[17] C. T. Yavuz, J. T. Mayo, W. W. Yu, A. Prakash, J. C. Falkner, S. J. Yeon, L. Cong, H. J. Shipley, A. Kan, M. Tomson, D. Natelson, and V. L. Colvin, Science **314**, 964 (2006).
[18] M. Zhang, Z. Zi, Q. Liu, P. Zhang, X. Tang, J. Yang, X. Zhu, Y. Sun, and J. Dai, Adv. Mater. Sci. Eng. **2013**, 609819 (2013).
[19] M. Aneja, A. Tovstolytkin, and G. S. Lotey, J. Magn. Magn. Mater. **442**, 423 (2017).
[20] Y. Zheng, H. Zhang, Y. Hu, L. Bai, and J. Xue, Int. J. Nanomedicine, **13**, 6177 (2018).